

Terahertz dielectric response and coupled dynamics of ferroelectrics and multiferroics from effective Hamiltonian simulations

Dawei Wang,¹ Jeevaka Weerasinghe,² Abdullah Albarakati,³ and L. Bellaiche⁴

¹*Electronic Materials Research Laboratory, Key Laboratory of the Ministry of Education and International Center for Dielectric Research, Xi'an Jiaotong University, Xi'an 710049, China*
dawei.wang@mail.xjtu.edu.cn

²*Physics Department, University of North Texas, Denton, Texas 76205, USA*
jeevaka.weerasinghe@unt.edu

³*Physics Department, The University College at Al-Gammom, Umm Al-Qura University Makkah, Saudi Arabia*
a_albrak@yahoo.com

⁴*Physics Department and Institute for Nanoscience and Engineering, University of Arkansas, Fayetteville, Arkansas 72701, USA*
laurent@uark.edu

Ferroelectric and multiferroic materials form an important class of functional materials. Over the last twenty years, first-principles-based effective Hamiltonian approaches have been successfully developed to simulate these materials. In recent years, effective Hamiltonian approaches were further combined with molecular dynamics methods to investigate *terahertz dynamical* properties of various perovskites. With this combination, a variety of ferroelectric and multiferroic materials, including BaTiO₃, Ba(Sr,Ti)O₃, Pb(Zr,Ti)O₃, BiFeO₃, and SrTiO₃ bulks and films have been simulated, which led to the understanding of complex phenomena and discovery of novel effects. In this review, we first provide technical details about effective Hamiltonians and molecular dynamics simulation. Then, we present applications of the combination of these two techniques to different perovskites. Finally, we also briefly discuss possible future directions of this approach.

PACS numbers:

I. INTRODUCTION

Ferroelectric materials have a spontaneous electric polarization that can be reversed by applying an external electric field. These compounds exhibit a wide range of important properties such as piezoelectricity, high dielectric constants and photoelectricity, which make them key materials for actuators, sensors, and potential candidates for energy conversion and storage¹⁻³. In recent years, multiferroic materials, which possess both spontaneous electric polarization and magnetic orders also attracted much attention⁴. Moreover, the continuing miniaturization of electronic devices has stimulated considerable research attention on ferroelectric and multiferroic nanostructures, such as ultrathin films and nanodots, which can have striking novel phenomena because of finite-size effects⁵.

The investigation of ferroelectric materials can be approximately divided into several stages. In 1920-1939, ferroelectricity were found in Rochelle salt type crystals (KDP as an example)⁶. Then, after the discovery of BaTiO₃ in the early 1940s, the number of studies on pure ferroelectric perovskites and solid solutions grow rapidly⁶⁻⁸. In the 1960s and 1970s, phenomenological Landau-type theories became widely used to investigate phase transitions of perovskites, where the essential idea is to express the free energy as Taylor expansions of order parameters⁹⁻¹¹. At approximately the same period, the soft mode theory for ferroelectrics was proposed and turned out to be very useful^{6,10,12-16}. Starting from the 1990s, the study of ferroelectric and multiferroic materials was accelerated by huge increase of computational capacity¹⁷ and subatomic scale observation techniques (e.g., high-resolution transmission electron microscopy)¹⁸⁻²¹.

On the theoretical side, the development of first-principles-based effective Hamiltonian approaches over the last 20 years proved to be quite useful to mimic and understand finite-temperature properties of perovskites (see Sec. II). More recently, these approaches were combined with molecular dynamics to predict complex dynamical properties of ferroelectrics and multiferroics, in the terahertz frequency range (see Sec. IV).

This review focuses on the combination of effective Hamiltonian approaches and molecular dynamics methods, in general, and on the prediction of properties resulting from its use, in particular. It is organized as follows. In Sec. II and III, we introduce the effective Hamiltonian approach and its implementation within the molecular dynamics method. In Sec. IV, we provide examples of the application of this approach to the investigation of several perovskites. Finally, in Sec. V, a summary is given and we invoke some possible future directions of this approach.

II. EFFECTIVE HAMILTONIAN SCHEMES, DEGREES OF FREEDOMS AND ENERGIES

Landau-type phenomenological theories have been used for more than 50 years to study ferroelectric materials, including their phase transitions²². On the other hand, the first microscopic, effective Hamiltonian approach of ferroelectric materials was only developed in the mid-nineties²³⁻²⁵ although the soft mode theory was known for a much longer time (see Refs.^{12,26} and references therein). Since then, it has achieved great successes in describing various ferroelectric materials^{24,25,27,29-31}. In a nutshell, effective Hamiltonian

methods first identify the most important degrees of freedom in a ferroelectric material, and then, based on symmetry arguments, construct the internal energy of the system as a function of these degrees of freedom and their interactions. The coefficients entering the effective Hamiltonian energy are typically obtained by *ab-initio* computations^{23,25}. Initially, only the so-called local modes and strains of simple systems were included in the effective Hamiltonian scheme^{24,25}. However, later on, alloy effects were added. For instance, an effective Hamiltonian scheme was developed to model (Ba,Sr)TiO₃ (BST) solid solutions for the whole compositional range³². Its total energy E_{tot} has two main terms:

$$E_{\text{tot}} = E_{\text{VCA}}(\{\mathbf{u}_i\}, \{v_i\}, \{\eta_H\}) + E_{\text{loc}}(\{\mathbf{u}_i\}, \{v_i\}, \{\eta_{\text{loc}}\}, \{\sigma_j\}) \quad (1)$$

where \mathbf{u}_i denotes the local soft mode centered on the Ti-site of the unit cell i (\mathbf{u}_i is directly proportional to the electric dipole of that cell); $\{v_i\}$ are the dimensionless displacement variables of the cell corners and are used to calculate inhomogeneous strain tensor components of the cell i ; $\{\eta_H\}$ is the homogeneous strain tensor, which allows the simulation supercell to vary in size and shape; σ_j characterizes the atomic configuration, with $\sigma_j=+1$ or -1 corresponding to the presence of a Ba or Sr atom, respectively, at the A-lattice site j ; and $\{\eta_{\text{loc}}\}$ represents the local strain resulting from the difference in ionic size between Ba and Sr atoms, which is relatively large ($\simeq 2\%$). E_{VCA} gathers the energy terms solely involving the local soft mode, strain and their mutual couplings resulting from the application of the virtual crystal approximation^{27,28,33} to model (Ba_{0.5}Sr_{0.5})TiO₃ solid solutions. On the other hand, E_{loc} can be thought of as a perturbative term due to the fact that BST systems possess real Ba and Sr atoms on the A-sites rather than a virtual, compositional-dependent $\langle A \rangle$ atom.

Antiferrodistortive (AFD) motions^{30,34} and magnetic degrees of freedom^{31,35} were also incorporated in some effective Hamiltonians. For instance, in the multiferroic BiFeO₃ material, the resulting effective Hamiltonian has a total energy that can be written as a sum of two main terms^{31,35,36}:

$$E_{\text{tot}} = E_{\text{FE-AFD}}(\{\mathbf{u}_i\}, \{\eta\}, \{\omega_i\}) + E_{\text{MAG}}(\{\mathbf{m}_i\}, \{\mathbf{u}_i\}, \{\eta\}, \{\omega_i\}), \quad (2)$$

where the ω_i pseudo-vector characterizes the tilting of oxygen octahedra in unit cell i of the investigated perovskite³¹ (see Fig. 1). Note that such tilting is also termed the antiferrodistortive (AFD) motion. \mathbf{m}_i is the magnetic dipole moment centered on the Fe-site i and has a fixed magnitude of $4\mu_B$ ³⁷. $E_{\text{FE-AFD}}$ is given in Ref.³⁰ and involves terms associated with ferroelectricity, strain and AFD motions, and their mutual couplings. E_{MAG} gathers magnetic degrees of freedom and their interactions with local modes, strains and oxygen octahedral tiltings, and is given in Refs.^{31,35,36}.

III. COMBINING MOLECULAR DYNAMICS AND EFFECTIVE HAMILTONIANS

Effective Hamiltonians can be put into Monte-Carlo (MC) algorithms (see, e.g. Refs.^{23,27,31}) or molecular dynamics (MD) simulations (see, e.g., Refs.^{38,39}), to predict material properties. A MC simulation generates configurations of a system with certain probabilities determined by their free energies at certain temperatures. The generated configurations are then used to find physical properties of the system statistically. The MC method has been put in use for finding static properties of ferroelectric materials since the introduction of the first effective Hamiltonian method²³. Examples include its application to BaTiO₃²³, Pb(Zr,Ti)O₃ solid solutions^{27,29,30} and BiFeO₃ multiferroics^{31,35,36,40}, for which the MC algorithm accurately predicted some important physical properties at finite temperature.

On the other hand, the effective-Hamiltonian-based MD method deals with the *dynamics* of the degrees of freedom directly, employing Newton's equation for the local modes, AFD motions and strains for ferroelectrics^{38,39}, and also the Landau-Lifshitz-Gilbert equation for magnetic moments⁴¹⁻⁴³ in multiferroics. This approach was used as early as the end of the 1990s to investigate KNbO₃ perovskites⁴⁴. Later, the method was further developed by Ponomareva *et al*³⁸ to obtain terahertz dielectric response of BaTiO₃ (which is a simple system where the two degrees of freedom of the effective Hamiltonian are local modes and strains). Surprisingly, two peaks (instead of only one single peak) were numerically found in the THz dielectric response³⁸. At this point, MD already shows its usefulness in understanding subtle phenomena. The effective-Hamiltonian-based MD method was further developed to include the dynamic variable related to AFD motions to investigate Pb(Zr,Ti)O₃^{39,45,71}. Recently the magnetic degree of freedom was also added into the combination of MD technique and effective Hamiltonians to investigate terahertz dynamical properties of multiferroics⁴³.

Combining MD and effective Hamiltonians has allowed the computation of complex dynamical properties, including dielectric responses^{38,39,43,45}, electrocaloric effect⁴⁶⁻⁴⁸, domain dynamics⁴⁹, the creation of electric field by dynamically altering the magnetic dipolar configurations in ferromagnets⁵⁰, and the investigation of BaTiO₃ thin-film capacitors⁵¹. Let us now describe in details this combination.

A. Dynamical equations obeyed by the structural degrees of freedom

The *structural* degrees of freedom of the effective Hamiltonian obey Newton's equation, that is:^{38,39}

$$M_{A_\alpha} \frac{d^2}{dt^2} A_\alpha = - \frac{\partial}{\partial A_\alpha} E_{\text{tot}}, \quad (3)$$

where A_α is one (Voigt or Cartesian) component of the aforementioned local modes, strains, and/or AFD vectors. E_{tot} is the internal energy provided by the effective Hamiltonian

scheme for the system under consideration (e.g. Eq. (2) for BiFeO_3). M_{A_α} has a dimension of a mass for the local modes and strains, while it can be interpreted as a moment of inertia when A_α is a Cartesian component of the AFD vectors. Note that, during the MD simulations^{38,39}, the temperatures of all these structural degrees of freedom are controlled by Evans-Hoover thermostats⁵².

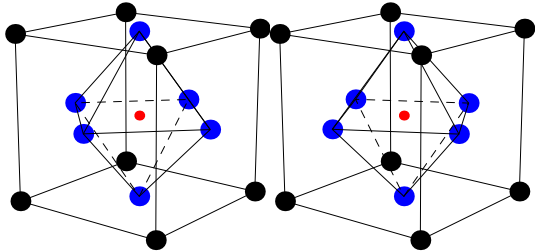


FIG. 1: For an ABO_3 system, the black dots (on the corners), red dots (in the center) and the blue dots (on the face centers) represent the A, B and oxygen atoms, respectively. The left panel shows the atoms at the ideal positions of the cubic phase, while the right panel shows the oxygen octahedron rotated around the pseudo-cubic [111].

B. Treating magnetic moments on a dynamical point of view

In multiferroic materials, such as BiFeO_3 , there exists yet another important degree of freedom: the magnetic moment. In contrast to the structural degrees of freedom, the dynamics of magnetic moments is described by the Landau-Lifshitz-Gilbert (LLG) equation⁴². The implementation and incorporation of LLG into MD simulations for multiferroics is not trivial since these simulations should also include the Newtonian dynamics followed by the structural degrees of freedom. This explains why many studies treat the magnetic moments and the structural degrees of freedom separately^{41,53,54}, showing the challenge of merging these two dynamics (even more so at finite temperature).

This merging was, in fact, accomplished in Ref.⁴³ for multiferroic BiFeO_3 using the effective Hamiltonian approach. For that, the stochastic Landau-Lifshitz-Gilbert (LLG) equation was implemented for the \mathbf{m}_i , the magnetic moment on unit cell i ⁴¹:

$$\frac{d\mathbf{m}_i}{dt} = -\gamma \mathbf{m}_i \times [\mathbf{B}_{\text{eff}}^i(t) + \mathbf{b}_{\text{fl}}^i(t)] - \gamma \frac{\lambda}{|\mathbf{m}_i| (1 + \lambda^2)} \mathbf{m}_i \times \{ \mathbf{m}_i \times [\mathbf{B}_{\text{eff}}^i(t) + \mathbf{b}_{\text{fl}}^i(t)] \}, \quad (4)$$

where $\mathbf{B}_{\text{eff}}^i = -\nabla_{\mathbf{m}_i} E_{\text{tot}}$ is the effective magnetic field acting on the i th magnetic moment, γ is the gyromagnetic ratio, λ is the damping coefficient. \mathbf{b}_{fl}^i is a fluctuation field that also acts on the i th magnetic moment, and allows to control the temperature of magnetic moments, as consistent with previous studies done on magnetic systems^{55,56}. The Box-Muller

method was used in Ref.⁴³ to generate random numbers obeying Gaussian distribution for \mathbf{b}_{fl}^i and to enforce the following conditions obeyed by this fluctuation field at the finite temperature, T ^{41,55}:

$$\langle \mathbf{b}_{\text{fl}}^i \rangle = 0, \quad (5)$$

$$\langle b_{\text{fl},\alpha}^i(t_1) b_{\text{fl},\beta}^i(t_2) \rangle = 2 \frac{\lambda k_B T}{\gamma |\mathbf{m}_i|} \delta_{\alpha,\beta} \delta(t_1 - t_2), \quad (6)$$

where α and β denote Cartesian coordinates and t_1 and t_2 are two different times. $\langle \rangle$ indicates an average over possible realizations of the fluctuating field⁴¹, $\delta_{\alpha,\beta}$ is the Kronecker delta function and $\delta(t_1 - t_2)$ is the Dirac delta function.

Note that (i) the LLG equation shown in Eq. (4), which contains the fluctuation field, is a Stratonovich stochastic differential equation⁴¹; and (ii) the semi-implicit method devised by Mentink *et al*⁵⁷ was adopted in Ref.⁴³ to properly integrate this LLG equation. This algorithm was found to be efficient and accurate enough for our investigations of multiferroics.

C. Obtaining dynamical responses via correlation function

For ferroelectric and multiferroic materials, the complex dielectric response, $\varepsilon_{\alpha\beta}(\nu)$, can be obtained via the proposed MD scheme in the gigahertz-terahertz regime at any temperature, using the following equation^{38,58,59}:

$$\varepsilon_{\alpha\beta}(\nu) - 1 = \frac{1}{\varepsilon_0 V k_B T} \left[\langle d_\alpha(t) d_\beta(t) \rangle + i 2\pi\nu \int_0^\infty dt e^{i2\pi\nu t} \langle d_\alpha(t) d_\beta(0) \rangle \right] \quad (7)$$

where ν is the frequency while α and β define Cartesian components and V is the volume of the chosen supercell, $\mathbf{d}(t)$ is the dipole moment of the system at time t , and $\langle \dots \rangle$ represents thermal averages.

Typically, each peak found in simulations in the spectra of $\varepsilon_{\alpha\beta}(\nu)$ is fitted by a classical harmonic oscillator

$$\varepsilon_{\alpha\beta}(\nu) = \frac{S\nu_r^2}{\nu_r^2 - \nu^2 + i\nu\gamma}, \quad (8)$$

where ν_r , γ and S are the resonant frequency, damping constant, and strength of the oscillator, respectively. In some cases (e.g., when a central mode exists), other spectra models have also been used⁶⁰.

Other type of dynamical responses can also be obtained. For example, one can replace the dipole moment by the magnetization or an AFD vector in Eq.(7) to predict the complex magnetic susceptibility⁴³ or the physical response of AFD vectors to their *ac* conjugate field, respectively.

IV. APPLICATIONS TO THE STUDY OF A VARIETY OF SYSTEMS

Having discussed the technical side of the effective-Hamiltonian MD approach for complex dynamical properties, we now show its application to ferroelectric and multiferroic materials via several examples.

A. Soft mode and central mode in BaTiO₃ and Ba(Sr,Ti)O₃ systems

BaTiO₃ is the first ferroelectric material that was studied in detail using the effective Hamiltonian method^{23,25}. It is therefore not surprising that the MD method was also first developed to obtain the complex dielectric response of BaTiO₃, which has “only” local modes and strains in the effective Hamiltonian. This “simple” system, however, gave rise to a surprise: it was numerically found that, for any temperature ranging between the Curie temperature T_C and 750 K (the system is in the paraelectric phase), a good fit of the dielectric response requires *two* classical damped harmonic oscillators rather than a single one³⁸. These two different overdamped modes of comparable strengths were found to contribute to the total dielectric response. The lower frequency mode softens as temperature approaches the Curie point from above. The higher-frequency mode softens less and stays in the 60–100 cm⁻¹ range and was found to be associated with temperature-independent short-range correlations.

Similar results were also found in (Ba_xSr_{1-x})TiO₃ with $x > 0.4$, but not in Pb(Zr_{0.4}Ti_{0.6})O₃³⁸. It was also found in the tetragonal ferroelectric phase of BaTiO₃⁵⁹. There, it was indicated that the low-frequency mode (which is often referred to as the “central mode”, CM) is related to the jumping of the local mode between different, but equivalent, potential minimum. This differs from the high-frequency mode, which is the well-known soft mode (SM) and that corresponds to dipolar oscillations around one energy minimum. Note that the CM in tetragonal BaTiO₃ was analyzed using a Debye relaxation model, and that the characteristic frequency of this mode was found to decrease as the temperature approaches T_C from below⁵⁹.

More recently, MD simulations also helped to elucidate the dielectric response in the paraelectric phase of (Ba, Sr)TiO₃ solid solutions, and to find whether the CM persists up to the highest temperatures, or rather if it disappears at some well-defined temperature T_{CM} that is higher than the Curie temperature^{61,62}. To account simultaneously for the SM and CM appearing in the dielectric response, the following equation was used^{59,63}:

$$\varepsilon(\nu) = \frac{S}{\nu_0^2 - \nu^2 - i\nu\Gamma - \delta^2/(1-i\nu/\nu_R)} \quad (9)$$

where S , ν_0 , Γ are the oscillator strength, frequency and damping constant of the SM, respectively; ν_R and δ are the relaxation frequency of the CM, and the coupling coefficient between the SM and CM, respectively. The MD results suggested that the coupling term δ is constant, while ν_R increases with temperature. Comparing three different models (that differ about the assumptions on the dependence of δ^2 and ν_R on temperature) to MD simulation results indicated a thermally activated dynamics of the coupling coefficient of CM-SM. It was shown that Eq. (9) can be used for all temperatures with well obtained parameters, and that the appearance of the CM in the dielectric spectra can be understood as a crossover between two regimes: a higher-temperature regime governed by the soft mode only (when $\nu_R \gg \delta^2/\Gamma$) *versus* a lower-

temperature regime exhibiting a coupled soft mode/central mode dynamics. The crossover temperature T_{CM} can be quantitatively determined from the fitting parameters of Eq. (9).

Moreover, the central mode had also been observed in SrTiO₃ films deposited on DyScO₃ substrates under tensile strain^{63,64} and was shown to have a strong effect on tunability⁶⁰ (see Sec. IV D).

B. Bilinear and nonlinear dynamical couplings in Pb(Zr,Ti)O₃

1. Bilinear coupling

In contrast to BaTiO₃, Pb(Zr,Ti)O₃ possesses antiferrodistortive oxygen octahedra tiltings that can strongly affect its properties. For example, it was shown that the correct Curie temperature can be obtained only when AFD is included as an independent degree of freedom in the effective Hamiltonian^{30,33}. Moreover, it was found that, below some critical temperature ($\simeq 200$ K, the exact value depends on the Ti composition), the AFD tiltings adopt a long-range order, which is described by the following two equations:

$$\langle \omega \rangle = \frac{1}{N} \sum_i \omega_i = 0, \quad (10)$$

$$\langle \omega_R \rangle = \frac{1}{N} \sum_i \omega_i (-1)^{n_x(i)+n_y(i)+n_z(i)} \neq 0. \quad (11)$$

where ω_i is the tilting angle of the oxygen octahedron at site i . These two equations show that, while the simple average of the tilting angle over the whole system is zero, the average associated with the R -point of the cubic Brillouin (i.e., multiplying by -1 when going from one B-site to any of its first nearest neighbor B sites) is finite.

Since an additional degree of freedom is identified in Pb(Zr,Ti)O₃, its dynamical coupling to the electric polarization is of interest. For instance, one can wonder if this coupling can give rise to additional peaks in Raman spectra or to other unexpected phenomena. An effective-Hamiltonian-based MD approach was further developed and exploited to address this important topic^{39,45}. First, the energy terms related to the AFD degree of freedom were incorporated in the MD program. Among others, the energy term representing the interaction energy between the local mode and AFD tiltings is given by

$$E_{\text{AFD-FE}} = \sum_i \sum_{\alpha,\beta,\gamma,\delta} D_{\alpha,\beta,\gamma,\delta} \omega_{i,\alpha} \omega_{i,\beta} u_{i,\gamma} u_{i,\delta}, \quad (12)$$

where i runs over all the unit cells and α, β, γ and δ denote Cartesian components, with the x , y , and z axes being chosen along the pseudocubic [100], [010], and [001] directions, respectively. The $D_{\alpha,\beta,\gamma,\delta}$ matrix elements quantify the couplings between local modes and AFD motions, and are extracted from local-density-approximation (LDA) calculations^{27,65}. Second, in addition to the dielectric response

of Eq. (7), the MD approach was also able to compute the following quantity:

$$\varepsilon_{\alpha\beta}^{\text{AFD}}(\nu) - 1 = \frac{1}{\varepsilon_0 V k_B T} \left[\langle \omega_{R,\alpha}(t) \omega_{R,\beta}(t) \rangle + i 2\pi\nu \int_0^\infty dt e^{i2\pi\nu t} \langle \omega_{R,\alpha}(t) \omega_{R,\beta}(0) \rangle \right], \quad (13)$$

where $\omega_R(t)$ are the order parameter vector associated with the AFD motions at the R -point of the cubic Brillouin zone³⁰ [see Eq. (11)] at time t and $\varepsilon_{\alpha\beta}^{\text{AFD}}(\nu)$ can be thought as the response of $\omega_R(t)$ to its ac conjugate field, which is a time-dependent staggered field. This physical response is then fitted by classical harmonic oscillators, which allows the identification of the natural resonant frequencies of the AFD motions.

Applying this newly developed MD approach to $\text{Pb}(\text{Zr}_{0.55}\text{Ti}_{0.45})\text{O}_3$, a cubic paraelectric phase was found for temperatures above the Curie temperature $T_C \sim 700$ K, and a $R3m$ phase, in which the polarization is along a $\langle 111 \rangle$ direction, exists between T_C and another critical temperature ~ 200 K. Below ~ 200 K, the oxygen octahedra tilting has a long-range ordering, rotating around the same $\langle 111 \rangle$ direction of the polarization, setting the system in the $R3c$ phase. These results are in good agreement with experiments^{66–68} and previous MC simulations³⁰. Then, the dielectric response of the system was obtained, and the resonant frequencies of the lowest-in-frequency dielectric peak [an $E(1\text{TO})$ mode], ν_r , were extracted. Such a mode represents dipolar oscillations perpendicular to the spontaneous polarization. Its frequency versus temperature follows the relation $\nu_r = C|T - T_C|^{1/2}$ close to T_C , which can be explained by Landau theory and which is an expected behavior. However, it was also found that two peaks, rather than a single $E(1\text{TO})$ peak, exist in the 50–70 cm^{-1} range for temperatures below ~ 200 K, which is the transition temperature at which the $R3m$ to $R3c$ phase transition occurs, which agrees well with Raman experimental findings^{69,70}.

In order to understand the origin of this additional mode, (i) the coupling between the local mode and AFD was switched off by setting $D_{\alpha,\beta,\gamma,\delta}$ to zero, resulting in only one dielectric peak remaining below ~ 200 K; (ii) the natural frequencies of oxygen octahedra tiltings were extracted from the analysis of Eq. (13), leading to the discovery that the AFD degree of free-

dom clearly has two natural frequencies in the 50–75 cm^{-1} range below 200 K that coincides with the two peaks observed in the dielectric response. These findings point to the fact that the coupling between the AFD and local mode is the reason for the additional peak below 200 K. Due to this coupling, the AFD acquires some polarity, while the “usual” E dielectric mode loses some polar character, resulting in the decrease of the electric dipole spectral weight below 200 K. When the system is in the $R3c$ phase or other similar phases ($\langle \mathbf{u} \rangle \neq 0$ and $\langle \omega_R \rangle \neq 0$, see below), the coupling between local mode and AFD motions can be expressed as

$$H_{\text{coupl,dynam}} \simeq \sum_i \kappa |\langle \mathbf{u} \rangle| |\langle \omega_R \rangle| \tilde{\mathbf{u}}_i \tilde{\omega}_i, \quad (14)$$

where $|\dots|$ denotes the magnitude of a vector, $\tilde{\mathbf{u}}_i$ (respectively, $\tilde{\omega}_i$) is the deviation of the local mode (respectively, AFD mode) in the unit cell i with respect to their spontaneous values. It was verified that the behavior of the spectra below 200 K can be understood by analyzing the dynamical equation for $\tilde{\mathbf{u}}_i$ under the influence of AFD, which is derived from the coupling of Eq. (14).

The effect of composition on the low-frequency modes at low temperature was also investigated⁷¹. At this point it is important to know that, within a small range of compositional variation (45%–56% Ti), the morphotropic boundary of $\text{Pb}(\text{Zr,Ti})\text{O}_3$ supports three low-temperature phases, namely rhombohedral $R3c$, monoclinic Cc , and tetragonal $I4cm$. This results in the rotation of the polarization from the $[111]$ to $[001]$ pseudo-cubic direction as the composition varies, which is the underlying reason why $\text{Pb}(\text{Zr,Ti})\text{O}_3$ has good performance in this region⁶⁶. Via the application of MD simulations, the number of low-frequency modes ($< 89 \text{ cm}^{-1}$), their resonant frequencies, and dielectric spectral weights were obtained to predict some characteristics of the low-frequency optical modes that can appear in the dielectric and Raman spectra at low temperature. Throughout this compositional range, both the local mode and AFD have long-range orders at low temperature, therefore the coupling of local mode and AFD is an important issue in analyzing the simulation results.

Practically, MD simulations were carried out for disordered PZT solid solutions, with Ti compositions ranging from 45.2% to 56.0% in intervals of 0.2% and for temperatures ranging from 1100K down to 10 K. The results are summarized in Table 1.

Ti Composition	45.2%–47.5%	47.5%–51.0%	51.0%–56.0%
Phase	rhombohedral $R3c$	monoclinic Cc	tetragonal $I4cm$
Number of modes	2 ^a	4 ^b	2 ^c
Origin	local mode and AFD ³⁹	local mode and AFD	local mode and AFD

TABLE I: Phases and low-frequency modes through the morphotropic boundary of $\text{Pb}(\text{Zr,Ti})\text{O}_3$ at 10K.

As indicated in Table 1, different phases have different number of modes. The $R3c$ phase has two modes ($E^{(1)}$ and $E^{(2)}$), the Cc phase has four modes ($A^{(1)}$, $A''^{(1)}$, $A^{(2)}$ and $A''^{(2)}$), and the $I4cm$ again has two modes ($E^{(1)}$ and $E^{(2)}$), which are consistent with group theory. It was found that the frequency differences between the A' and A'' modes originating from $E^{(1)}$ and $E^{(2)}$, are largest near the compositional midpoint of the Cc phase (that is located around a Ti composition of 49.4%) and decrease to either side of it. That is, the splitting of the E mode in the monoclinic phase depends on how strong the phase is monoclinic, which can be quantified by the monoclinic depth parameter defined in Eq. (4) of Ref.⁷¹. Analytical model was constructed, based on the coupling of Eq. (12), to fit the frequencies of each mode and understand the variation of spectra weight with respect to Ti composition at different phases. In particular, the splitting in the Cc phase can be fitted with monoclinic depth as a fitting parameter. Such analytical models were able to accurately reproduce characteristics of the low-frequency optical modes and led to a better understanding of the coupling between ferroelectric and AFD degrees of freedom.

2. Nonlinear coupling

The coupling between the local mode and AFD as shown in Eq. (12) is not limited to the linear part. As a matter of fact, the nonlinear coupling can also have important effects on the spectra⁴⁵. Let us consider a structural phase that has a spontaneous polarization but no long-range AFD order, which is true above the AFD phase transition temperature. To simplify the investigation of the dynamics of \mathbf{u}_i and ω_i due to their non-linear couplings, we introduce $\tilde{\mathbf{u}}_i$ and $\tilde{\omega}_i$ such as:

$$\begin{cases} \mathbf{u}_i(t) = \langle \mathbf{u} \rangle + \tilde{\mathbf{u}}_i(t) \\ \omega_i(t) = \langle \omega_{\mathbf{R}} \rangle + \tilde{\omega}_i(t) = \tilde{\omega}_i(t) \end{cases}, \quad (15)$$

In the above equation, t represents time and $\tilde{\mathbf{u}}_i$ (respectively, $\tilde{\omega}_i$) is the deviation of the local mode (respectively, AFD mode) in the unit cell i with respect to its spontaneous value $\langle \mathbf{u} \rangle$ (respectively, $\langle \omega_{\mathbf{R}} \rangle$), and $\langle \omega_{\mathbf{R}} \rangle$ is the R point average [see Eq. (11)] oxygen octahedra tilting, which is zero in the temperature range of investigation. Plugging Eq. (15) into Eq. (12), it can be shown that the most important coupling term has the following form:

$$H_{\text{coupl,dynam}} = \sum_i \kappa \langle u \rangle \tilde{u}_i (\tilde{\omega}_i)^2, \quad (16)$$

and the dynamical equation for \tilde{u}_i is:

$$\frac{d^2 \tilde{u}_i}{dt^2} = -4\pi^2 (\nu_r^{\text{FE}})^2 \tilde{u}_i - \frac{\kappa \langle u \rangle}{m_u} (\tilde{\omega}_i)^2 + \frac{Z^* E(t)}{m_u}, \quad (17)$$

^aTwo (double degenerate) E modes.

^bThe degeneracy between the E modes is lifted.

^cTwo (double degenerate) E modes.

where ν_r^{FE} is the natural frequency of the local mode when there is no coupling with AFD and m_u is the local mode effective mass. $E(t)$ is an applied ac electric field. Equation (17) shows the existence of a coupling between the square of the AFD displacement and the displacement of the local mode. One can prove that when ν_r^{FE} is close to *twice* the AFD resonance frequency, Eq. (17) leads to *two* resonant frequencies given by $\nu_r^2 = \nu_{\text{FE}}^2 \pm \Omega^2$, where Ω^2 depends on the κ coupling parameter, as well as, on the value of the spontaneous polarization, $\langle u \rangle$.

The nonlinear coupling shown in Eq. (16) induces novel dynamical phenomenon in $\text{Pb}(\text{Zr,Ti})\text{O}_3$ solid solutions: in the simulations, two A_1 modes appear at a temperature that coincides with the temperature for which the frequency of the single A_1 mode equals twice of that of the AFD natural frequency. These two modes persist for lower temperature. This unexpected doubling of the A_1 mode was confirmed by Raman scattering techniques⁴⁵, and is a signature of the so-called Fermi resonance, which occurs when the frequency of one dynamical variable is close to the first overtone of another dynamical variable⁷².

C. Terahertz Dynamics of multiferroic BiFeO_3

With the addition of magnetic moments as another dynamical degree of freedom, multiferroic BiFeO_3 is a complicated system. Using the method detailed in Sec. III B, we performed first-principles-based MD simulations on this system, for the spin-canted antiferromagnetic structure (rather than the magnetic cycloid)⁴³.

The first important problem to address when dealing with the stochastic LLG equation is to find the damping constant λ of Eq. (4). This can be achieved by comparing the MD results to those of MC. It was numerically found that, at any temperature, λ has little effect on the spontaneous polarization and oxygen octahedra tilting, therefore yielding MD results being similar to the MC predictions for these structural properties for a wide range of damping coefficients. However, the effect of λ can be clearly seen when investigating magnetic properties in the multiferroic BFO – as consistent with the fact that λ “only” appears in the spin equations of motions. It was found that a wide range of λ (namely, $1.0 \times 10^{-4} \leq \lambda \leq 1.0 \times 10^{-1}$) leads to a satisfactory agreement (i.e., a difference of less than 3%) between the MD and MC results at any temperature for the magnetic structure. A large range of λ can therefore be adopted to obtain equilibrated properties, which makes the MD approach suitable to model different multiferroic/ferromagnetic bulks or nanostructures that may have very different damping constants due to different damping mechanisms⁴².

We then chose $\lambda = 1.0 \times 10^{-4}$ and computed the complex electric and magnetic susceptibilities of BiFeO_3 using equations similar to Eq. (7). A fixed temperature of 20 K was selected, for which the crystallographic equilibrium state is

R3c and both the electric and magnetic susceptibilities were obtained. Four resonance peaks were found in the dielectric susceptibility, having resonant frequencies of 151 cm^{-1} , 176 cm^{-1} , 240 cm^{-1} and 263 cm^{-1} . They correspond to E , A_1 , E and A_1 symmetries, respectively (note that these are not all the modes appearing in measured Raman or infrared spectra⁷³⁻⁸¹ due to the limited number of degrees of freedom included in the effective Hamiltonian). The first two (lowest-in-frequency) peaks were found to be mostly related to the sole FE degree of freedom incorporated in the effective Hamiltonian scheme, while the last two peaks have also a significant contribution from AFD distortions – as consistent with Ref. [82]. As revealed in Refs.^{39,71} and explained in Sec. IV B 1, bilinear couplings between the FE and AFD modes in the *R3c* phase allow the AFD mode to acquire some polarity, which explains why these last two peaks emerge in the dielectric spectra.

Moreover, two peaks can be seen in the *magnetic* susceptibility, their predicted resonant frequencies being $\sim 7\text{ cm}^{-1}$ and $\sim 85\text{ cm}^{-1}$, respectively. Since none of the frequencies coincides with the dielectric resonant frequencies, it was concluded that they are not electromagnons, but rather “solely” magnons. Moreover, the lowest-in-frequency magnon entirely disappears when the spin-canted structure was intentionally removed in BiFeO_3 by switching off a specific parameter in the simulation. Tracking the motions of both the ferromagnetic and antiferromagnetic vectors, the lowest-in-frequency magnon was found to be associated with the rotation of magnetic dipoles inside the (111) plane (that contains the polarization), which is consistent with Refs.^{83,84}. The second magnetic peak is associated with fast oscillations of the magnetic dipoles going in-and-out of the (111) plane, as well as, a change in length of the weak FM vector. This second peak therefore corresponds to the so-called optic antiferromagnetic mode of Ref.⁸⁵ and to the high-frequency gapped mode of Ref.⁸⁴. Examining the relation between the second peak and the coupling between magnetic moments and other structural dynamical variables, the abnormally large frequency of the second peak was numerically found to originate from *static* couplings between the \mathbf{m}_i 's and structural variables, with these couplings generating a large magnetic anisotropy. It was further found that AFD distortions can significantly affect the resonant frequency of this second magnetic peak.

D. Effect of the central mode on dielectric tunability of ferroelectrics

Dielectric tunability is an important quantity to measure how the dielectric constant of a material responds to an applied direct-current (*dc*) electric field. Large dielectric tunability near room temperature in GHz/THz range is important for many technological applications, such as lens antennas, phased array radars, and tunable filters, etc. To reveal the connection between tunability and internal dynamics, the effective-Hamiltonian-based MD approach was applied to the study of SrTiO_3 (STO) bulk and strained films (under a tensile strain of $\simeq 1.6\%$)⁶⁰. In the MD simulations, $12 \times 12 \times 12$ or

$14 \times 14 \times 14$ supercells were used for temperatures being in the interval of 900-130 K, starting from high temperature and cooling down the systems. In agreement with experiments⁹³, there is no phase transition for STO bulk in this temperature range. For the strained STO film, however, the *Amm2* orthorhombic phase (with a polarization pointing along the in-plane [110] direction) was found to occur below $T_c \sim 305\text{ K}$, which is consistent with measurements^{64,94}.

The complex dielectric response was first obtained at different direct current (*dc*), which was then used to compute the tunability, $\tau(E, \nu)$, of STO bulk at a given frequency ν , for each biased *dc* electric field \mathbf{E} , following the formula:

$$\tau(E, \nu) = \frac{\text{Re}[\varepsilon_{\alpha\beta}(0, \nu)]}{\text{Re}[\varepsilon_{\alpha\beta}(\mathbf{E}, \nu)]} \quad (18)$$

where $\text{Re}[\varepsilon_{\alpha\beta}(0, \nu)]$ and $\text{Re}[\varepsilon_{\alpha\beta}(\mathbf{E}, \nu)]$ are the real parts of the complex dielectric functions for no bias field and under a *dc* field E , respectively, at the frequency ν .

At 300 K, the tunability of STO bulk was obtained, which is relatively low ($\sim 7\%$) and in good agreement with spectroscopic measurements⁹⁵. The tunability obtained from MD simulations was then fitted using Landau-Devonshire-theory-based phenomenological formulas⁹⁶. For low fields, the formula is

$$\tau(E) = 1 + \beta(\varepsilon_0\varepsilon(0))^3 E^2, \quad (19)$$

and for high fields the formula is

$$\tau(E) = 3(\varepsilon_0\varepsilon(0))\beta^{\frac{1}{3}}E^{\frac{2}{3}} \quad (20)$$

where $\varepsilon(0)$ is the zero-field static dielectric constant, ε_0 is the permittivity of free space, and β is a fitting coefficient, which also appears in the energy expansion in the Landau-Devonshire theory. For STO bulk, the low-field value of β (to be denoted by β_L) was found to be nearly equal to its high-field value (to be referred to as β_H), and both of them are close to experimentally extracted values of Ref.⁹⁵⁻⁹⁷.

Similar MD simulations were performed at 320K for the epitaxially strained STO films under a *dc* field applied along the pseudo-cubic [110] direction to compare with experiments^{63,94}. It is found that there are two peaks in the in-plane ε_{xx} dielectric response when no bias field is applied, which are the CM and the SM, as consistent with time-domain THz spectroscopy measurements^{63,64}. The STO film was found to have a very large tunability near room temperature^{63,96,98}. What is surprising is that the low fields ($E < 4\text{ MV/m}$) value β_L is two orders of magnitude smaller than β_H in the film. This significant difference indicates that the Landau-Devonshire theory cannot adequately predict tunability of epitaxially strained STO films under low fields. It was verified that such deviation originates from the existence of the CM in the STO film, which makes the dielectric response of a system obeyed Eq. (9) rather than Eq. (8). Similar results were also found in the dielectric tunability of disordered $(\text{Ba}_{0.5}\text{Sr}_{0.5})\text{TiO}_3$ solid solution (that also possesses a CM in its paraelectric phase⁹⁹) at 270 K and at $\nu=10\text{ GHz}$. The results of STO film and $(\text{Ba}_{0.5}\text{Sr}_{0.5})\text{TiO}_3$ bulk therefore show

that, in the presence of a CM, the Landau-Devonshire theory cannot be reasonably applied for fitting tunabilities. A new equation is necessary for fitting the tunability of STO epitaxial films and other systems exhibiting CM in general. Using Eq. (9), it is shown analytically that, when CM exists, a quartic term in electric field is necessary to qualitatively represent the influence of the CM mode on the tunability. Therefore, the tunability is given by a polynomial of order 4:

$$\tau_2(E, 0) \simeq 1 + d_1 E + d_2 E^2 + d_3 E^4, \quad (21)$$

where the E^3 term was numerically found to be negligible.

V. CONCLUSION

In this work, we have demonstrated that the effective-Hamiltonian-based molecular dynamics simulation approach is a useful tool for investigating dynamical properties of perovskites. Via examples of BaTiO_3 , $\text{Pb}(\text{Zr},\text{Ti})\text{O}_3$, BiFeO_3 and SrTiO_3 , we have shown that the dielectric responses and tunabilities are closely connected to the internal dynamics and inherent microscopic couplings.

Let us finish this review by discussing what possible future research problems may be tackled using the combination of molecular dynamics and effective Hamiltonian schemes.

First of all, the investigation of dynamical properties of multiferroics just started. There are therefore a flurry of activities to be done in that direction. For instance, it may be interesting to take a close look at the terahertz electric and magnetic dynamics of BFO when the magnetic ordering consists of the known cycloid. It may be that this magnetic ordering does lead to the formation of the so-called electromagnons since it is supposed to give rise to many magnetic peaks that are equally spaced in frequency and which can then overlap with dielectric peaks⁸⁶⁻⁸⁸. It would also be exciting to find the *dynamical* magneto-electric coefficients, that is the parameters quantifying how the application of an *ac* magnetic field (respectively, electric field) affects the time-dependent electric polarization (respectively, magnetization).

Second, another field of study may be to investigate the terahertz dynamics of the so-called ferroelectric relaxors. Some

typical signatures of a ferroelectric relaxor are that its *ac* dielectric response peaks at certain temperature, with the position of the peak changing with frequency, while the system remains paraelectric and cubic down to the lowest temperature. Note that one well known relaxor, namely the so-called PMN-PT, had been investigated with the MD method, but based on the bond-valence model⁸⁹⁻⁹¹ rather than effective Hamiltonian. On the other hand, an effective Hamiltonian for another specific relaxor, namely disordered $\text{Ba}(\text{Zr}_{0.5},\text{Ti}_{0.5})\text{O}_3$ (BZT) solid solutions, had been shown to generate many of its anomalous properties⁹². In particular, it was shown that BZT contains polar nanoregions. Revealing the dynamics of these regions should lead to a better knowledge of relaxors, and the MD method described above may be very useful to reach such goal.

Furthermore, first-principles-based simulations recently predicted the unusual formation of a vortex structure for their electrical dipoles below a critical temperature in some ferroelectrics¹⁰⁰⁻¹⁰², which was also experimentally observed^{19,20,103,104}. Using molecular dynamics simulations coupled with effective Hamiltonians to reveal the terahertz dynamics of such formation is also a promising avenue to pursue in a near future.

We thus hope that the use of the effective Hamiltonian within molecular dynamics simulations will lead to the discoveries of various effects in a near future, and will continue to enrich our understanding of complex dynamical phenomena.

Acknowledgements

This work is financially supported by NSF DMR-1066158. L.B. also acknowledges the Department of Energy, Office of Basic Energy Sciences, under contract ER-46612, ONR Grants N00014-11-1-0384 and N00014-12-1-1034, and ARO Grant W911NF-12-1-0085 for discussions with scientists sponsored by these grants. D.W. acknowledges support from the National Natural Science Foundation of China under Grant No. 51272204.

¹ B.-K. Lai, I. Ponomareva, I. A. Kornev, L. Bellaiche, and G. Salamo, *Phys. Rev. B* **75**, 85412 (2007)

² S. Prosandeev and L. Bellaiche, *Phys. Rev. B* **75**, 94102 (2007).

³ H. Ogihara, C. Randall, and S. Trolier-McKinstry, *J. Am. Ceram. Soc.* **92**, 1719 (2009).

⁴ N. A. Spaldin, S.-W. Cheong, and R. Ramesh, *Physics Today* **63**, 38 (2010).

⁵ G. Catalan, J. Seidel, R. Ramesh, and J. F. Scott, *Rev. Mod. Phys.* **84**, 119 (2012).

⁶ L. E. Cross and R. E. Newnham, *History of Ferroelectrics*, reprinted from *Ceramics and Civilization, Volume III, High-Technology Ceramics – Past, Present, and Future* (The American Ceramic Society, Westerville, Ohio, 1987).

⁷ M. Dove, *Am. Mineral.* **82**, 213 (1997).

⁸ M. Vijatovic, J. Bobic, and B. Stojanovic, *Sci. Sinter.* **40**, 155 (2008).

⁹ M. Lines and A. Glass, *Principles and Applications of Ferroelectrics and Related Materials* (Clarendon Press, Oxford, 1977).

¹⁰ A. D. Bruce and R. Cowley, *Structural Phase Transitions* (Taylor and Francis, London, 1981).

¹¹ E. Salje, *Phase transitions in ferroelastic and co-elastic crystals* (Cambridge University Press, Cambridge, 1993).

¹² W. Cochran, *Phys. Rev. Lett.* **3**, 412 (1959).

¹³ W. Cochran, *Adv. Phys.* **9**, 387 (1960).

¹⁴ R. Blinc and B. Zeks, *Soft Modes in Ferroelectrics and Antiferroelectrics* (North Holland, Amsterdam, 1974).

¹⁵ J. Scott, *Rev. Mod. Phys.* **46**, 83 (1974).

¹⁶ W. Cochran, *Ferroelectrics* **35**, 3 (1981).

- ¹⁷ S. R. Phillpot, S. B. Sinnott, and A. Asthagiri, *Annu. Rev. Mater. Res.* **37**, 239 (2007).
- ¹⁸ C.-L. Jia, S.-B. Mi, K. Urban, I. Vrejoiu, M. Alexe, and D. Hesse, *Nat. Mater.* **7**, 57 (2008).
- ¹⁹ C.-L. Jia, K. W. Urban, M. Alexe, D. Hesse, and I. Vrejoiu, *Science* **331**, 1420 (2011).
- ²⁰ C. T. Nelson, B. Winchester, Y. Zhang, S.-J. Kim, A. Melville, C. Adamo, C. M. Folkman, S.-H. Baek, C.-B. Eom, D. G. Schlom, L.-Q. Chen, and X. Pan, *Nano Lett.* **11**, 828 (2011).
- ²¹ M. Rossell, R. Erni, M. Prange, J.-C. Idrobo, W. Luo, R. Zeches, S. Pantelides, and R. Ramesh, *Phys. Rev. Lett.* **108**, 1 (2012).
- ²² P. Chandra, P. B. Littlewood, K. Rabe, C. H. Ahn, and J.-M. Triscone, *Physics of Ferroelectrics: A Modern Perspective* (Springer-Verlag Berlin, Heidelberg, 2007).
- ²³ W. Zhong, D. Vanderbilt, and K. Rabe, *Phys. Rev. Lett.* **73**, 1861 (1994).
- ²⁴ R. King-Smith, and D. Vanderbilt, *Phys. Rev. B* **49**, 5828 (1994).
- ²⁵ W. Zhong, D. Vanderbilt, and K. M. Rabe, *Phys. Rev. B* **52**, 6301 (1995).
- ²⁶ R. Cowley, *Phys. Rev. Lett.* **9**, 159 (1962).
- ²⁷ L. Bellaiche and D. Vanderbilt, *Phys. Rev. B* **61**, 7877 (2000).
- ²⁸ N. J. Ramer and A. M. Rappe, *J. Phys. Chem. Solids* **61**, 317 (2000).
- ²⁹ L. Bellaiche, A. Garcia, and D. Vanderbilt, *Ferroelectrics* **266**, 41 (2002).
- ³⁰ I. Kornev, L. Bellaiche, P. Janolin, B. Dkhil, and E. Suard, *Phys. Rev. Lett.* **97**, 157601 (2006).
- ³¹ I. Kornev, S. Lisenkov, R. Haumont, B. Dkhil, and L. Bellaiche, *Phys. Rev. Lett.* **99**, 227602 (2007).
- ³² L. Walizer, S. Lisenkov, and L. Bellaiche, *Phys. Rev. B* **73**, 144105 (2006).
- ³³ L. Bellaiche, A. García, and D. Vanderbilt, *Phys. Rev. Lett.* **5427**(2000).
- ³⁴ D. Vanderbilt and W. Zhong, *Ferroelectrics* **206**, 181 (1998).
- ³⁵ D. Albrecht, S. Lisenkov, W. Ren, D. Rahmedov, I. A. Kornev, and L. Bellaiche, *Phys. Rev. B* **81**, 140401(R) (2010).
- ³⁶ D. Rahmedov, D. Wang, J. Íñiguez, and L. Bellaiche, *Phys. Rev. Lett.* **109**, 037207 (2012).
- ³⁷ J. Neaton, C. Ederer, U. Waghmare, and N. Spaldin, *Phys. Rev. B* **71**, 014113 (2005).
- ³⁸ I. Ponomareva, L. Bellaiche, T. Ostapchuk, J. Hlinka, and J. Petzelt, *Phys. Rev. B* **77**, 012102 (2008).
- ³⁹ D. Wang, J. Weerasinghe, L. Bellaiche, and J. Hlinka, *Phys. Rev. B* **83**, 020301(R) (2011).
- ⁴⁰ S. Prosandeev, D. Wang, W. Ren, J. Íñiguez, and L. Bellaiche, *Adv. Funct. Mater.* **23**, 234 (2013).
- ⁴¹ J. García-Palacios and F. Lázaro, *Phys. Rev. B* **58**, 14937 (1998).
- ⁴² T. L. Gilbert, *IEEE Trans. Magn.* **40**, 3443 (2004).
- ⁴³ D. Wang, J. Weerasinghe, and L. Bellaiche, *Phys. Rev. Lett.* **109**, 067203 (2012).
- ⁴⁴ H. Krakauer, R. Yu, C.-Z. Wang, and K. M. Rabe **3779** (1999).
- ⁴⁵ D. Wang, E. Buixaderas, Jorge Íñiguez, J. Weerasinghe, Hong Wang, and L. Bellaiche, *Phys. Rev. Lett.* **107**, 175502 (2011).
- ⁴⁶ S. Lisenkov and I. Ponomareva, *Phys. Rev. B* **80**, 140102 (2009).
- ⁴⁷ S. Beckman, L. Wan, J. a. Barr, and T. Nishimatsu, *Mater. Lett.* **89**, 254 (2012).
- ⁴⁸ I. Ponomareva and S. Lisenkov, *Phys. Rev. Lett.* **108**, 167604 (2012).
- ⁴⁹ Q. Zhang, R. Herchig, and I. Ponomareva, *Phys. Rev. Lett.* **107**, 177601 (2011).
- ⁵⁰ S. Prosandeev and L. Bellaiche, *Phys. Rev. Lett.* **102**, 097205 (2009).
- ⁵¹ T. Nishimatsu, U. Waghmare, Y. Kawazoe, and D. Vanderbilt, *Phys. Rev. B* **78**, 104104 (2008).
- ⁵² D. Evans, W. Hoover, B. Failor, B. Moran, and A. Ladd, *Phys. Rev. A* **28**, 1016 (1983).
- ⁵³ P.-W. Ma, C. Woo, and S. Dudarev, *Phys. Rev. B* **78**, 024434 (2008).
- ⁵⁴ P.-W. Ma, S. Dudarev, A. Semenov, and C. Woo, *Phys. Rev. E* **82**, 031111 (2010).
- ⁵⁵ W. Brown, *Phys. Rev.* **130**, 1667 (1963).
- ⁵⁶ R. Kubo and N. Hashitsume, *Prog. Theor. Phys. Suppl.* **46**, 210 (1970).
- ⁵⁷ J. H. Mentink, M. V. Tretyakov, a. Fasolino, M. I. Katsnelson, and T. Rasing, *J. Phys.: Condens. Matter* **22**, 176001 (2010).
- ⁵⁸ J. Caillol, D. Levesque, and J. Weis, *J.Chem. Phys.* **85**, 6645 (1986).
- ⁵⁹ J. Hlinka, T. Ostapchuk, D. Nuzhnyy, J. Petzelt, P. Kuzel, C. Kadlec, P. Vanek, I. Ponomareva, and L. Bellaiche, *Phys. Rev. Lett.* **101**, 167402 (2008).
- ⁶⁰ J. Weerasinghe, D. Wang, and L. Bellaiche, *J. Phys: Condens. Matter* **25**, 252202 (2013).
- ⁶¹ T. Ostapchuk, J. Petzelt, J. Hlinka, V. Bovtun, P. Kužel, I. Ponomareva, S. Lisenkov, L. Bellaiche, a. Tkach, and P. Vilarinho, *J. Phys.: Condens. Matter* **21**, 474215 (2009).
- ⁶² J. Weerasinghe, L. Bellaiche, T. Ostapchuk, P. Kužel, C. Kadlec, S. Lisenkov, I. Ponomareva, and J. Hlinka, *MRS Commun.* **3**, 41 (2013).
- ⁶³ C. Kadlec, F. Kadlec, H. Němec, P. Kužel, J. Schubert, and G. Panaitov, *J. Phys.: Condens. Matter* **21**, 115902 (2009).
- ⁶⁴ D. Nuzhnyy, J. Petzelt, S. Kamba, P. Kužel, C. Kadlec, V. Bovtun, M. Kempa, J. Schubert, C. M. Brooks, and D. G. Schlom, *App. Phys. Lett.* **95**, 232902 (2009).
- ⁶⁵ P. Hohenberg and W. Kohn, *Phys. Rev.* **155**, B864 (1964).
- ⁶⁶ B. Jaffe, W. Cook, and H. Jaffe, *Piezoelectric Ceramics* (Academic, London, 1971).
- ⁶⁷ B. Noheda, D. E. Cox, G. Shirane, R. Guo, B. Jones, and L. E. Cross, *Phys. Rev. B* **63**, 014103 (2000).
- ⁶⁸ B. Noheda, L. Wu, and Y. Zhu, *Phys. Rev. B* **66**, 060103 (2002).
- ⁶⁹ D. Bäuerle and A. Pinczuk, *Solid State Commun.* **19**, 1169 (1976).
- ⁷⁰ M. Deluca, H. Fukumura, N. Tonari, C. Capiani, N. Hasuike, K. Kisoda, C. Galassi, and H. Harima, *J. Raman Spectros.* **42**, 488 (2011).
- ⁷¹ J. Weerasinghe, D. Wang, and L. Bellaiche, *Phys. Rev. B* **85**, 014301 (2012).
- ⁷² E. Fermi, *Z. Phys.* **71**, 250 (1931).
- ⁷³ R. Haumont, J. Kreisel, P. Bouvier, and F. Hippert, *Phys. Rev. B* **73**, 132101 (2006).
- ⁷⁴ S. Kamba, D. Nuzhnyy, M. Savinov, J. Šebek, J. Petzelt, J. Prokleška, R. Haumont, and J. Kreisel, *Phys. Rev. B* **75**, 024403 (2007).
- ⁷⁵ H. Fukumura, S. Matsui, H. Harima, T. Takahashi, T. Itoh, K. Kisoda, M. Tamada, Y. Noguchi, and M. Miyayama, *J. Phys.: Condens. Matter* **19**, 365224 (2007).
- ⁷⁶ R. Lobo, R. Moreira, D. Lebeugle, and D. Colson, *Phys. Rev. B* **76**, 172105 (2007).
- ⁷⁷ D. Rout, K.-S. Moon, and S.-J. L. Kang, *J. Raman Spectros.* **40**, 618 (2009).
- ⁷⁸ J. Lu, M. Schmidt, P. Lunkenheimer, A. Pimenov, A. A. Mukhin, V. D. Travkin, and A. Loidl, *J. Phys.: Conf. Ser.* **200**, 012106 (2010).
- ⁷⁹ R. Palai, J. F. Scott, R. S. Katiyar, and H. Schmid, *Phys. Rev. B* **81**, 064110 (2010).
- ⁸⁰ A. A. Porporati, K. Tsuji, M. Valant, A.-K. Axelsson, and G. Pezzotti, *J. Raman Spectros.* **41**, 84 (2010).
- ⁸¹ J. Hlinka, J. Pokorny, S. Karimi, and I. Reaney, *Phys. Rev. B* **83**, 020101(R) (2011).

- ⁸² P. Hermet, M. Goffinet, J. Kreisel, and P. Ghosez, *Phys. Rev. B* **75**, 220102(R) (2007).
- ⁸³ P. Pincus, *Phys. Rev.* **5**, 13 (1960).
- ⁸⁴ R. de Sousa and J. E. Moore, *App. Phys. Lett.* **92**, 022514 (2008).
- ⁸⁵ K. L. Livesey and R. L. Stamps, *Phys. Rev. B* **81**, 094005 (2010).
- ⁸⁶ A. B. Sushkov, M. Mostovoy, R. V. Aguilar, S.-W. Cheong, and H. D. Drew, *J. Phys.: Condens. Matter* **20**, 434210 (2008).
- ⁸⁷ A. Pimenov, A. M. Shuvaev, A. A. Mukhin, and A. Loidl, *J. Phys.: Condens. Matter* **20**, 434209 (2008).
- ⁸⁸ A. Pimenov, A. Shuvaev, A. Loidl, F. Schrettle, A. A. Mukhin, V. D. Travkin, V. Y. Ivanov, and A. M. Balbashov, *Phys. Rev. Lett.* **102**, 107203 (2009).
- ⁸⁹ Y.-H. Shin, V. Cooper, I. Grinberg, and A. Rappe, *Phys. Rev. B* **71**, 054104 (2005).
- ⁹⁰ I. Grinberg, Y.-H. Shin, and A. Rappe, *Phys. Rev. Lett.* **103**, 197601 (2009).
- ⁹¹ H. Takenaka, I. Grinberg, and A. M. Rappe, *Phys. Rev. Lett.* **110**, 147602 (2013).
- ⁹² A. R. Akbarzadeh, S. Prosandeev, E. J. Walter, a. Al-Barakaty, and L. Bellaiche, *Phys. Rev. Lett.* **108**, 257601 (2012).
- ⁹³ V. V. Lemanov, E. P. Smirnova, P. P. Syrnikov, and E. A. Tarakanov, *Phys. Rev. B* **54**, 3151(1996).
- ⁹⁴ J.H. Haeni, P. Irvin, W. Chang, R. Uecker, P. Reiche, Y.L. Li, S. Choudhury, W. Tian, M.E. Hawley, B. Craigo, A.K. Tagantsev, X.Q. Pan, S.K. Streiffer, L.Q. Chen, S.W. Kirchoefer, J. Levy and D.G. Schlom, *Nature*, **430**, 758 (2004).
- ⁹⁵ V. Skoromets, F. Kadlec, C. Kadlec, H. Němec, I. Rychetsky, G. Panaitov, V. Müller, D. Fattakhova-Rohlfing, P. Moch, and P. Kužel, *Phys. Rev. B* **84**, 174121 (2011).
- ⁹⁶ A. K. Tagantsev, V.O. Sherman, K.F. Astafiev, J. Venkatesh and N. Setter, *J. Electroceram.* **11**, 5 (2003).
- ⁹⁷ P. Kužel, F.Kadlec, *Comptes Rendus Physique*, **9**, 197 (2008).
- ⁹⁸ P. Kužel, F. Kadlec, J. Petzelt, J. Schubert and G. Panaitov, *Appl. Phys. Lett.* **91** 232911 (2007).
- ⁹⁹ S. Lisenkov, I. Ponomareva and L. Bellaiche, Conference proceedings (IEEE), DOD HPCMP, 2011 Users Group Conference (2011).
- ¹⁰⁰ I. I. Naumov, L. Bellaiche, and H. Fu, *Nature* **432**, 737 (2004).
- ¹⁰¹ D. Sichuga and L. Bellaiche, *Phys. Rev. Lett.* **106**, 196102 (2011).
- ¹⁰² L. Louis, I. Kornev, G. Geneste, B. Dkhil, and L. Bellaiche, *J. Phys.: Condens. Matter* **24**, 402201 (2012).
- ¹⁰³ Y. Ivry, D. P. Chu, J. F. Scott, and C. Durkan, *Phys. Rev. Lett.* **104**, 1 (2010).
- ¹⁰⁴ R. G. P. McQuaid, L. J. McGilly, P. Sharma, a. Gruverman, and J. M. Gregg, *Nat. Commun.* **2**, 404 (2011).